High-pressure behaviour of Prussian blue analogues: interplay of hydration, Jahn-Teller distortions and vacancies

SUPPLEMENTARY INFORMATION

Hanna L. B. Boström,[a] Ines E. Collings,[b] Andrew B. Cairns,[b,c] Carl P. Romao[a,d] and Andrew L. Goodwin*[a]

[a] Department of Chemistry, University of Oxford, Inorganic Chemistry Laboratory, South Parks Road, Oxford OX1 3QR, U.K.

[b] European Synchrotron Radiation Facility, 71 Avenue des Martyrs, 38000 Grenoble, France.

[c] Department of Materials, Imperial College London, Royal School of Mines, Exhibition Road, SW7 2AZ, UK.

[d] Institut für Anorganische Chemie, Universität Tübingen, Auf der Morgenstelle 18, 72076 Tübingen, Germany.

*To whom correspondence should be addressed; E-mail: andrew.goodwin@chem.ox.ac.uk

Contents

1 Variable-pressure lattice parameters **3**

2 Birch-Murnaghan fits **8**

3 Single crystal X-ray diffraction of $Mn[Co(CN)_6]_{0.67}$ **11**

4 Crystallographic details **15**

5 Phase transitions in $Cu[Pt(CN)_6]$ **22**

6 References **22**

1 Variable-pressure lattice parameters

Table S1: Assigned space groups, unit cell parameters and unit cell volumes for $Mn[Co(CN)_6]_{0.67}$ as a function of pressure. Horizontal lines demarcate data collected from different crystals. Entries marked "**P**" were refined by Pawley refinement of wide-angle scans, and asterisks denote data collected on decompression. Estimated uncertainty is ±0.1 GPa at all pressures.

p (GPa)	Space group	a (Å)	c (Å)	V (Å^3)
0.00	$Fm\bar{3}m$	10.4197(3)		1131.27(11)
0.13 **P**	$Fm\bar{3}m$	10.3817(2)		1118.93(7)
0.30 **P**	$Fm\bar{3}m$	10.3418(2)		1106.08(7)
0.55	$Fm\bar{3}m$	10.2891(2)		1089.26(7)
1.03	$Fm\bar{3}m$	10.1689(4)		1051.52(7)
0.13	$Fm\bar{3}m$	10.4048(2)		1126.42(7)
0.30	$Fm\bar{3}m$	10.36565(17)		1113.76(5)
0.77	$Fm\bar{3}m$	10.26071(15)		1080.27(5)
1.03	$Fm\bar{3}m$	10.1933(3)		1059.12(10)
1.31	$Fm\bar{3}m$	10.1457(5)		1044.35(15)
0.13	$Fm\bar{3}m$	10.3964(4)		1123.69(13)
1.65	$R\bar{3}$	7.2070(7)	16.942(3)	762.1(2)
1.86	$R\bar{3}$	7.1799(4)	16.8416(15)	751.88(10)
2.10	$R\bar{3}$	7.1596(4)	16.7625(15)	744.13(10)
1.99 *	$R\bar{3}$	7.1647(3)	16.7956(13)	746.65(9)
1.78 *	$R\bar{3}$	7.1795(4)	16.8670(17)	752.94(11)
1.61 *	$R\bar{3}$	7.1964(4)	16.9344(15)	759.50(10)
1.52 *	$R\bar{3}$	7.2018(3)	16.9754(15)	762.48(10)
1.31 *	$R\bar{3}$	7.2295(5)	17.089(2)	773.5(16)
1.20 *	$R\bar{3}$	7.2329(5)	17.128(2)	776.00(14)
0.99 *	$R\bar{3}$	7.2524(4)	17.2638(17)	786.38(11)
0.79 *	$Fm\bar{3}m$	10.1935(5)		1059.17(15)
0.60 *	$Fm\bar{3}m$	10.2744(4)		1084.58(13)
0.33 *	$Fm\bar{3}m$	10.3486(4)		1108.28(13)
0.14 *	$Fm\bar{3}m$	10.3998(5)		1124.81(14)

Table S2: Assigned space groups, unit cell parameters and unit cell volumes for $Cu[Co(CN)_6]_{0.67}$ as a function of pressure. Asterisks denote data collected on decompression. Estimated uncertainty is ±0.1 GPa at all pressures unless otherwise stated.

p (GPa)	Space group	a (Å)	V (Å^3)
0.00	$Fm\bar{3}m$	10.0648(2)	1019.57(7)
0.08	$Fm\bar{3}m$	10.0587(2)	1017.70(7)
0.22	$Fm\bar{3}m$	10.0430(2)	1012.94(7)
0.43	$Fm\bar{3}m$	10.0226(3)	1006.79(8)
0.64	$Fm\bar{3}m$	10.00371(2)	1001.113(7)
0.94	$Fm\bar{3}m$	9.9814(4)	994.43(10)
1.18	$Fm\bar{3}m$	9.9624(4)	988.76(11)
1.43	$Fm\bar{3}m$	9.9416(4)	982.58(12)
1.71	$Fm\bar{3}m$	9.9173(4)	975.38(11)
1.90	$Fm\bar{3}m$	9.9001(4)	970.32(11)
2.11	$Fm\bar{3}m$	9.8818(4)	964.95(13)
2.31	$Fm\bar{3}m$	9.8658(5)	960.27(14)
2.47	$Fm\bar{3}m$	9.8531(5)	956.6(2)
2.96	$Fm\bar{3}m$	9.8207(4)	947.17(13)
3.27	$Fm\bar{3}m$	9.8075(6)	943.4(2)
1.6(6) *	$Fm\bar{3}m$	9.9823(9)	994.7(3)
0.22 *	$Fm\bar{3}m$	10.0643(4)	1019.41(13)

Table S3: Assigned space groups, unit cell parameters and unit cell volumes for $Mn[Pt(CN)_6]$ as a function of pressure. Asterisks denote data collected on decompression. Estimated uncertainty is ± 0.1 GPa at all pressures.

p (GPa)	Space group	a (Å)	c (Å)	V (Å^3)
0.00	$Fm\bar{3}m$	10.75251(3)		1243.166(12)
0.09	$Fm\bar{3}m$	10.74336(3)		1239.995(12)
0.27	$Fm\bar{3}m$	10.72786(4)		1234.636(13)
0.57	$Fm\bar{3}m$	10.70046(3)		1225.201(12)
0.86	$Fm\bar{3}m$	10.67324(3)		1215.876(11)
1.02	$Fm\bar{3}m$	10.65777(4)		1210.594(13)
1.21	$Fm\bar{3}m$	10.63443(4)		1202.659(13)
1.41	$R\bar{3}$	6.3858(4)	19.163(3)	676.75(15)
1.58	$R\bar{3}$	6.3324(4)	19.140(4)	664.7(2)
1.75	$R\bar{3}$	6.2955(4)	19.089(3)	655.22(14)
1.88	$R\bar{3}$	6.2757(4)	19.095(4)	651.3(2)
2.10	$R\bar{3}$	6.2426(3)	19.054(3)	643.05(11)
2.23	$R\bar{3}$	6.2253(3)	19.029(3)	638.67(12)
2.34	$R\bar{3}$	6.2119(3)	19.012(3)	635.34(12)
2.44	$R\bar{3}$	6.2014(4)	18.995(3)	632.63(12)
2.61	$R\bar{3}$	6.1874(4)	18.963(3)	628.73(12)
0.91 *	$Fm\bar{3}m$	10.66944(4)		1214.58(2)
0.39 *	$Fm\bar{3}m$	10.72270(4)		1232.857(13)

Table S4: Assigned space groups, unit cell parameters and unit cell volumes for $Cu[Pt(CN)_6]$ as a function of pressure. Asterisks denote data collected on decompression. Estimated uncertainty is ± 0.1 GPa at all pressures.

p (GPa)	Space group	$\sqrt{2}a$ (Å)	c (Å)	V (Å^3)
0.00	$I4/mmm$	10.29225(2)	11.03503(6)	584.472(5)
0.10	$I4/mmm$	10.28616(2)	11.01782(5)	582.870(4)
0.21	$I4/mmm$	10.28017(2)	10.99938(5)	581.218(4)
0.36	$I4/mmm$	10.27264(3)	10.97484(7)	579.071(6)
0.51	$I4/mmm$	10.26496(5)	10.94564(13)	576.667(10)
0.69	$I4/mmm$	10.25704(7)	10.9146(2)	574.146(16)
0.94	$I4/mmm$	10.24554(9)	10.8807(3)	571.08(2)
0.29 *	$I4/mmm$	10.2850(4)	10.9801(13)	580.75(9)

2 Birch-Murnaghan fits

Variable-pressure unit cell volumes were fitted for all phases across the full stability range to second-order Birch-Murnaghan (B-M) equation of states (EoS) using EOSFitGUI.[S1] In all cases the estimated uncertainty in refined volumes and pressure ($\sigma_p = \pm 0.1$ GPa) were included in the fitting procedure. As for the fits to lattice parameters presented in the main text, only volumes refined on compression were fitted except for the high pressure phase of $Mn[Co(CN)_6]_{0.67}$ where decompression points were included due to (i) the low number of points collected on compression and (ii) the very small hysteresis observed. For all other cases hysteresis was observed however all phase transitions were reversible.

For the four compounds studied here we find no statistically significant deviation from second-order B-M behaviour. This is determined by inspection of the fits to $p(V)$ data (Figure S1), the uncertainties of refined parameters, and by inspection of the f–F plots[†] (Figure S2). As noted in the main text, visual inspection of the low pressure phase of $Mn[Pt(CN)_6]$ may suggest softening on increasing pressure, however such fits are not robust. Here we present both second and third-order fits for completeness; refined B-M parameters are included in all cases in Figure S2.

[†]For an f–F plot, a horizontal trend (within error) suggests data is best accounted for using a second-order B-M fit; a straight line with a positive or negative gradient suggests the derivative of the bulk modulus $B' \neq 4$, and so a third-order fit is appropriate; where non-straight line behaviour is observed higher order fits may be used if a sufficient number of data points have been recorded.[S2]

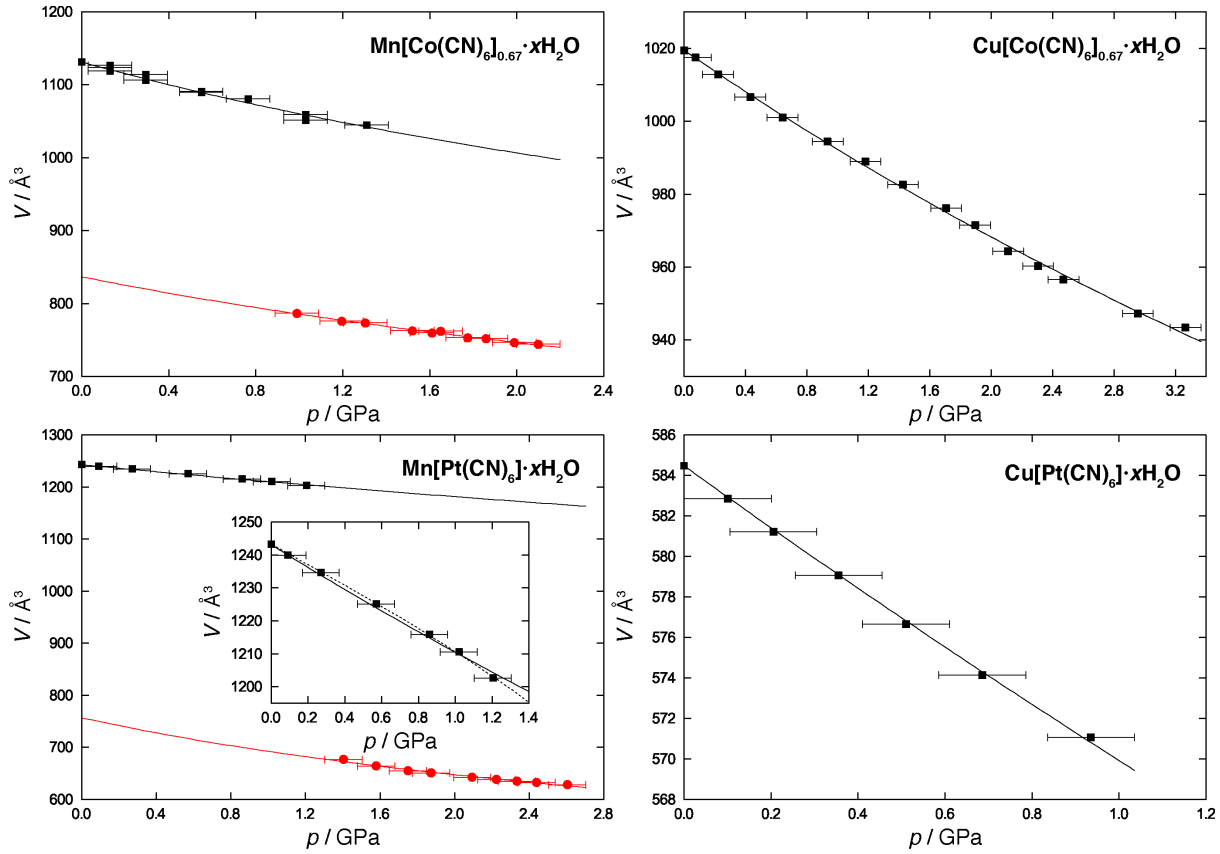

Figure S1: Fits to experimental unit cell volumes using 2$^{\mathrm{nd}}$-order Birch-Murnaghan EoS using EOSFitGUI for each compound studied. In each case, black squares indicate the low-pressure phase and red circles the high-pressure phase; open markers indicate data collected on decompression. Fits to data are given by the black and red curves respectively and for the low-pressure phase of Mn[Pt(CN)$_6$] second and third-order fits are shown for comparison by the solid line and dashed curves in the inset.

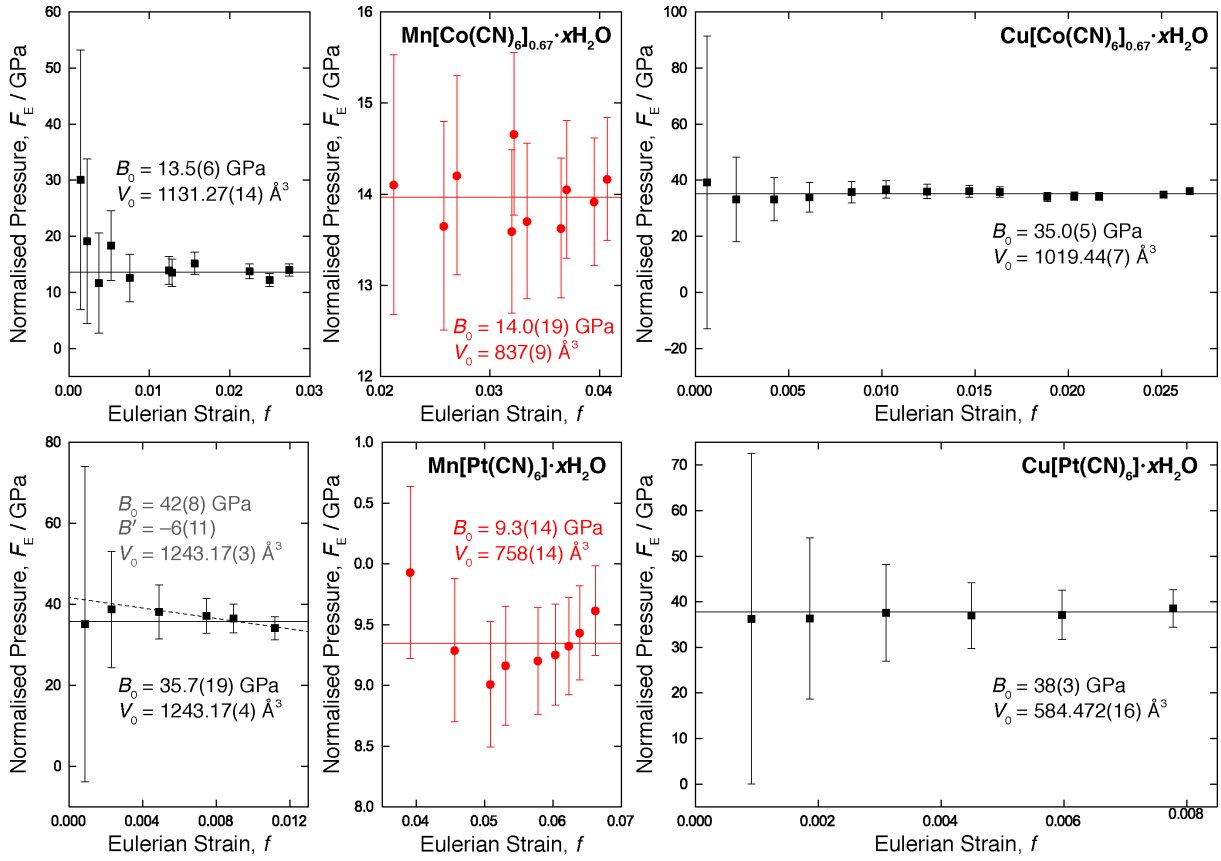

Figure S2: Plots of Eulerian strain (f) *vs.* normalised pressure (F_{E}) using a second-order Birch-Murnaghan EoS fit for each compound studied. The high and low-pressure phases are shown in separate panels where a phase transition is observed, with black squares indicating the low-pressure phase and red circles the high-pressure phase; open markers indicate data collected on decompression. Fits to data are given by the black and red lines respectively and for the low-pressure phase of Mn[Pt(CN)$_6$], second and third-order fits are shown for comparison by the solid line and dashed lines.

3 Single crystal X-ray diffraction of $Mn[Co(CN)_6]_{0.67}$

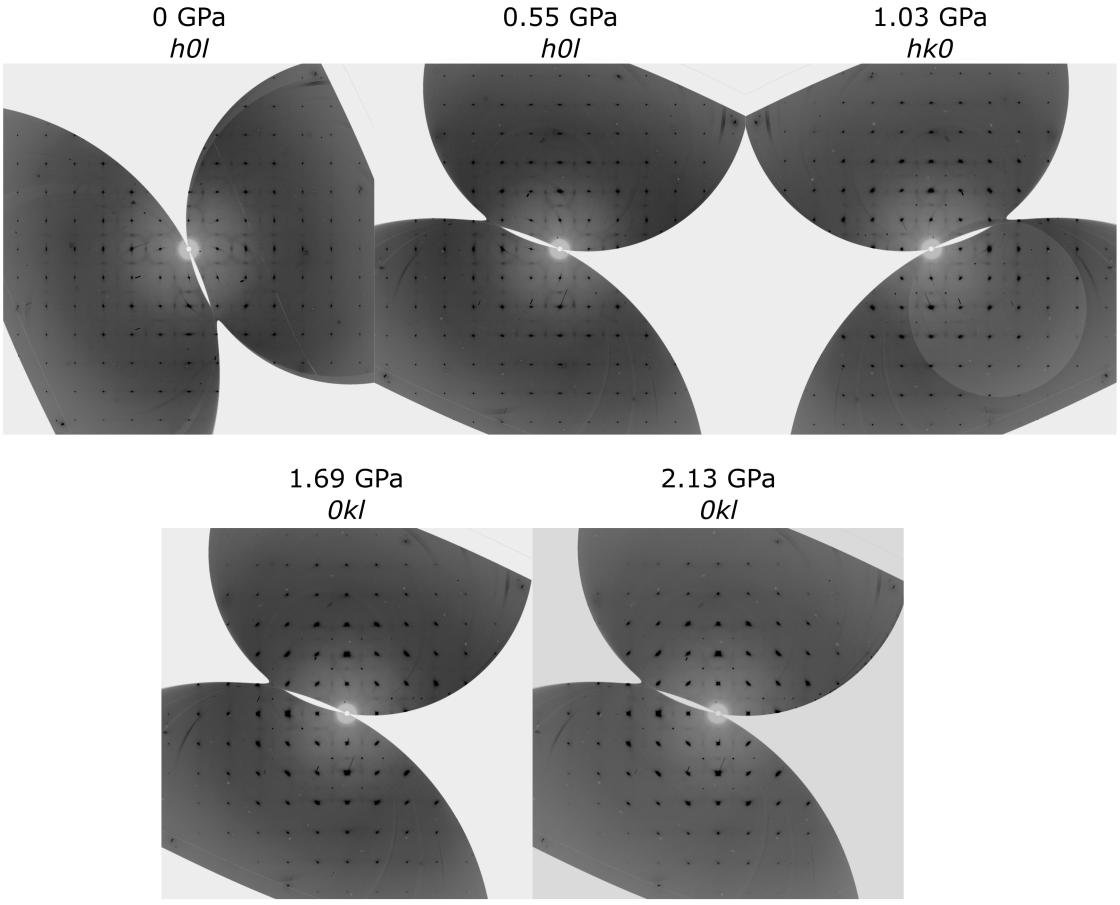

Figure S3: Reciprocal space reconstructions of one crystal of $Mn[Co(CN)_6]_{0.67}$ under pressure. Note that because of increased exposure to the X-ray beam, this particular crystal did not undergo a phase transition, but the shape of the diffraction peaks is different at 1.70 and 2.1 GPa within the high-pressure phase region. The diffuse scattering does not significantly change with pressure.

Table S5: Twin domain relations for $Mn[Co(CN)_6]_{0.67}$-II that are classified by the rotation of the unit cell along a specific axis in reciprocal space. The $twin_1$ cell is in red, $twin_2$ in blue, $twin_3$ in green, and $twin_4$ in purple as depicted in Figures S4 and S5.

Relation	rotation (°)	reciprocal axis
$twin_1$ and $twin_2$	120	[0.7 0 0.7]
$twin_1$ and $twin_4$	120	[001]
$twin_3$ and $twin_4$	240	[0.7 0 0.7]

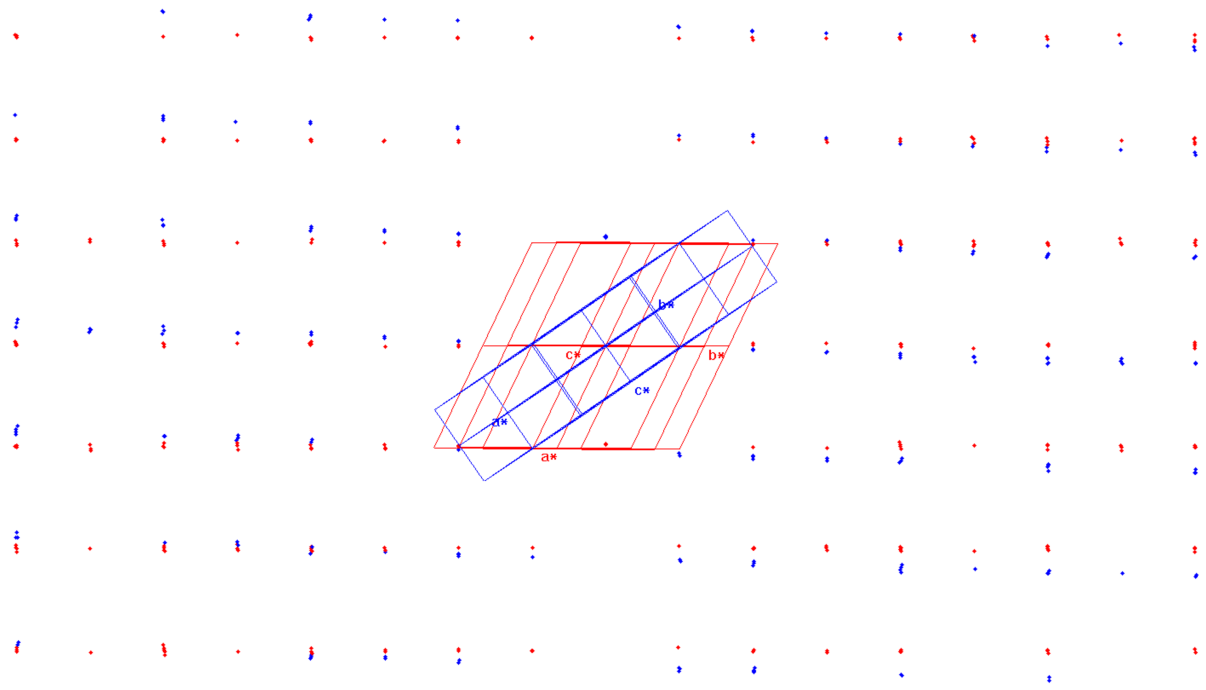

Figure S4: The first two most intense twin lattices of $Mn[Co(CN)_6]_{0.67}$-II in red and blue with the corresponding reciprocal space reflections as viewed in *CrysAlisPro*.[S?]

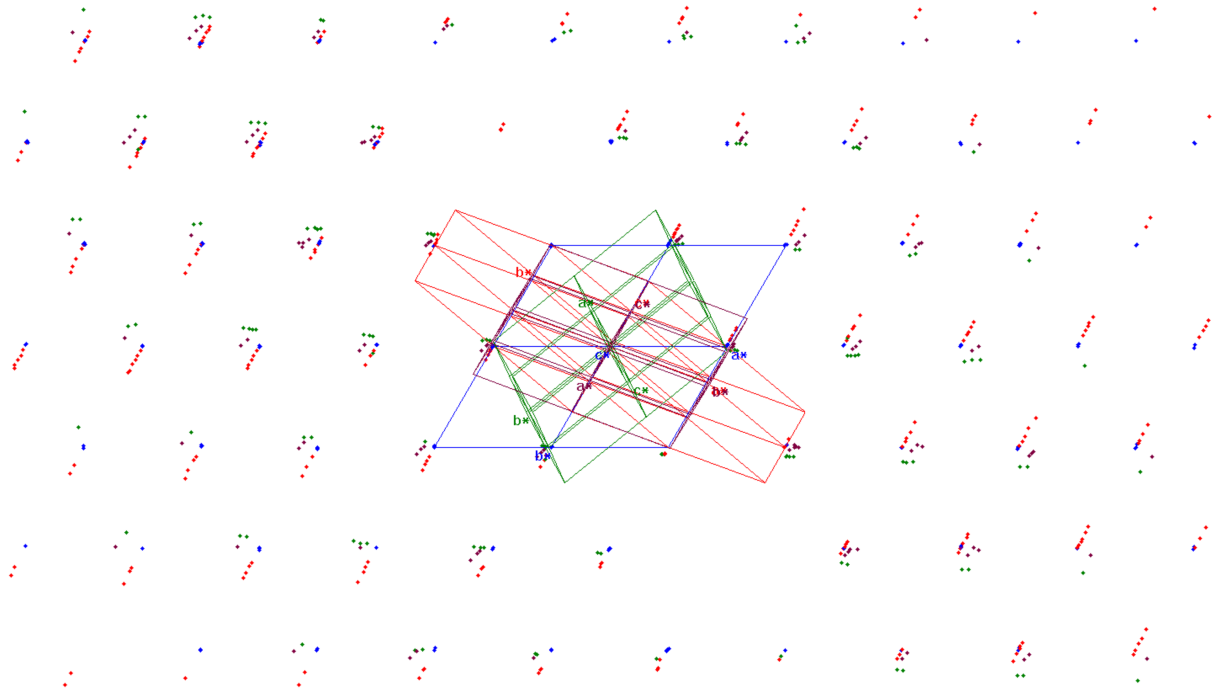

Figure S5: The twin lattices of $Mn[Co(CN)_6]_{0.67}$-II in red, blue, green, and purple with the corresponding reciprocal space reflections as viewed in *CrysAlisPro*.[S?]

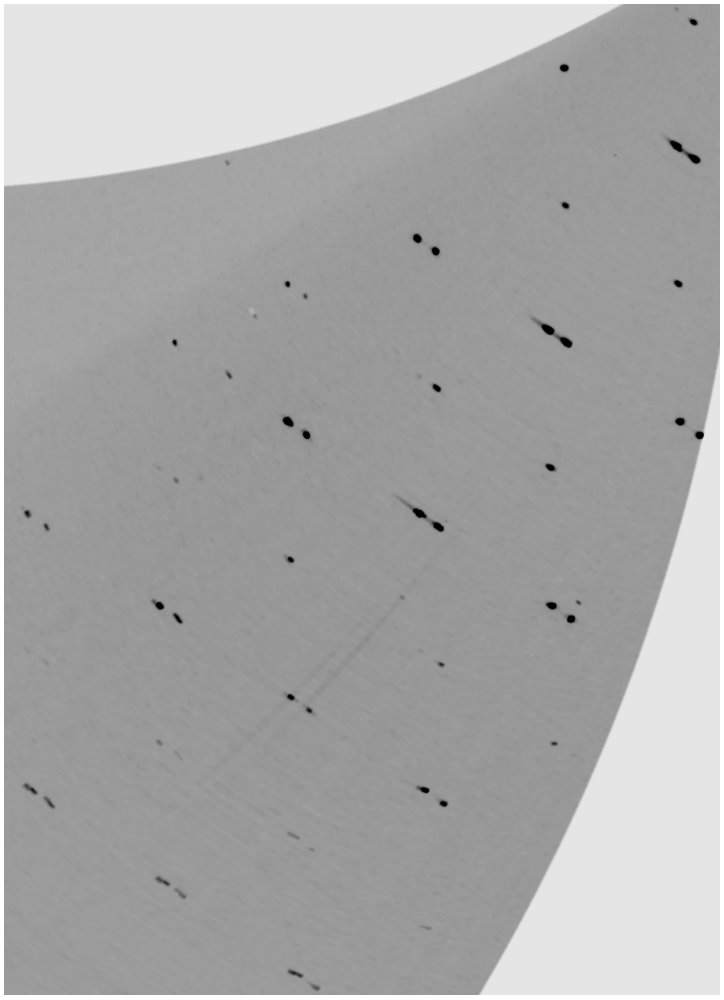

Figure S6: The $h3l$ plane in reciprocal space for the Mn[Co(CN)$_6$]$_{0.67}$-II phase at 1.65 GPa, where the two most intense twin domains can be observed (twin$_1$ and twin$_2$).

4 Crystallographic details

Table S6: Crystallographic details determined by single crystal X-ray diffraction for $Mn[Co(CN)_6]_{0.67}$-I at 0 GPa. The thermal parameters were refined anisotropically for C and N and isotropically for all other atoms. The thermal parameters for H are 1.2 times those of the O atoms.

Formula	$MnCo_{0.67}C_4N_4{\cdot}2(H_2O)$
M_w (g mol^{-1})	234.39
Crystal system	cubic
Space group	$Fm\bar{3}m$
Z	4
a (Å)	10.4197(3)
V (Å^3)	1131.27(11)
X-ray wavelength (Å)	0.41115
Crystal colour	colourless
No. of reflections measured	1047
Unique reflections	161
Unique with $I > 2\sigma$	117
$R_{\rm int}$	0.0463
No. of refined parameters	11
R_1 [I $> 2\sigma$(I)]	0.0394
wR_2 (all data)	0.1257
$\Delta\rho_{\rm max}, \Delta\rho_{\rm min}$ (e$^-$Å^{-3})	0.458, −0.517

Atom	occ	x	y	z	$U_{\rm iso}$ (Å^2)
Mn	1	0.0	0.5	0.0	0.0277(5)
Co	$\frac{2}{3}$	0.0	0.0	0.0	0.0201(5)
C	$\frac{2}{3}$	0.0	0.1800(7)	0.0	0.0385(15)
N	$\frac{2}{3}$	0.0	0.2930(8)	0.0	0.066(2)
O	1	0.25	0.25	0.25	0.29(3)
H	$\frac{1}{2}$	0.302(6)	0.198(6)	0.302(6)	0.353

Table S7: Crystallographic details determined by single crystal X-ray diffraction for $Mn[Co(CN)_6]_{0.67}$-II at 1.7(1) GPa. The thermal parameters were refined isotropically for O and anisotropically for all other atoms. Hydrogen atoms were omitted.

Formula	$MnCo_{0.67}C_4N_4{\cdot}2H_2O$
M_w (g mol^{-1})	234.39
Crystal system	rhombohedral
Space group	$R\bar{3}$
Z	3
a (Å)	7.2026(15)
c (Å)	16.964(7)
V (Å^3)	762.1(4)
Radiation (Å)	0.41112
Crystal colour	colourless
No. of reflections measured	378
Unique reflections	312
Unique with $I > 2\sigma$	195
$R_{\rm int}$	0.0347
No. of refined parameters	26
R_1 [I $> 2\sigma$(I)]	0.0894
wR_2 (all data)	0.2508
$\Delta\rho_{\rm max}, \Delta\rho_{\rm min}$ (e$^-$Å^{-3})	0.790, −0.500

Atom	occ	x	y	z	$U_{\rm iso}$ (Å^2)
Mn	1	$\frac{1}{3}$	$\frac{2}{3}$	$\frac{1}{6}$	0.0666(19)
Co	$\frac{2}{3}$	$\frac{2}{3}$	$\frac{1}{3}$	$\frac{1}{3}$	0.0387(15)
C	$\frac{2}{3}$	0.463(4)	0.398(4)	0.2632(13)	0.059(4)
N	$\frac{2}{3}$	0.404(4)	0.465(4)	0.2349(13)	0.076(5)
O	1	0.0	0.0	0.2509(15)	0.109(6)

Table S8: Crystallographic details determined by powder X-ray diffraction for $Mn[Pt(CN)_6]$-I at 0 GPa. The C–N distance was restrained to 1.13 Å, the Mn–N distance to 2.20 Å and the Pt–C distance to 2.04 Å, in agreement with Ref. 3.

Formula		$MnPtC_6N_6$			
Space group		$Fm\bar{3}m$			
a (Å)		10.75250(6)			
Z		4			
R_{wp}		0.781%			
Atom	occ	x	y	z	B_{iso} (Å^2)
Pt	1	0.0	0.0	0.0	3.506(10)
Mn	1	0.0	0.5	0.0	3.506
C	1	0.0	0.5	0.3059(2)	3.506
N	1	0.0	0.5	0.2032(2)	3.506

Table S9: Crystallographic details determined by powder X-ray diffraction for $Mn[Pt(CN)_6]$-I at 1.2(1) GPa. The C–N distance was restrained to 1.13 Å, the Mn–N distance to 2.20 Å and the Pt–C distance to 2.04 Å, in agreement with Ref. 3.

Formula		$MnPtC_6N_6$			
Space group		$Fm\bar{3}m$			
a (Å)		10.63443(4)			
Z		4			
R_{wp}		0.733%			
Atom	occ	x	y	z	B_{iso} (Å^2)
Pt	1	0.0	0.0	0.0	3.61(10)
Mn	1	0.0	0.5	0.0	3.61
C	1	0.0	0.5	0.3057(2)	3.61
N	1	0.0	0.5	0.2002(3)	3.61

Table S10: Crystallographic details determined by powder X-ray diffraction for $Mn[Pt(CN)_6]$-II at 1.4(1) GPa. The C–N distance was restrained to 1.13 Å, Mn–N distance to 2.0 Å and the Pt–C distance to 2.0 Å. Thermal parameters were fixed to the values from the ambient phase.

Formula		$MnPtC_6N_6$			
Space group		$R\bar{3}$			
a (Å)		6.3748(3)			
c (Å)		19.170(2)			
Z		3			
R_{wp}		1.177%			
Atom	occ	x	y	z	B_{iso} (Å^2)
Mn	1	$\frac{1}{3}$	$\frac{2}{3}$	$\frac{1}{6}$	3.5
Pt	1	$\frac{2}{3}$	$\frac{1}{3}$	$\frac{1}{3}$	3.5
C	1	0.4301(9)	0.3317(12)	0.2620(4)	3.5
N	1	0.3207(10)	0.4054(8)	0.2352(4)	3.5

Table S11: Crystallographic details determined by powder X-ray diffraction for $Cu[Pt(CN)_6]$ at 0 GPa. The positions of the C and N atoms could not be refined robustly, so were fixed to values to give sensible bond lengths.

Formula		$CuPtC_6N_6$			
Space group		$I4/mmm$			
a (Å)		7.27774(5)			
c (Å)		11.03537(12)			
Z		2			
R_{wp}		0.555%			
Atom	occ	x	y	z	B_{iso} (Å^2)
Cu	1	0.0	0.0	0.0	3.76(6)
Pt	1	0.5	0.5	0.0	3.76
C1	1	0.0	0.0	0.318	3.76
N1	1	0.0	0.0	0.216	3.76
C2	1	0.304	0.304	0.0	3.76
N2	1	0.194	0.194	0.0	3.76

Table S12: Crystallographic details determined by powder X-ray diffraction for $Cu[Co(CN)_6]_{0.67}$ at 0 GPa. The C–N distance was restrained to 1.13 Å, Cu–N distance to 2.15 Å and the Co–C distance to 2.03 Å.

Formula	$CuCo_{0.67}C_4N_4$				
Space group	$Fm\bar{3}m$				
a (Å)	10.0634(2)				
Z	4				
R_{wp}	0.813%				
Atom	occ	x	y	z	B_{iso} (Å^2)
Cu	1	0.0	0.5	0.0	1.7(2)
Co	$\frac{2}{3}$	0.0	0.0	0.0	1.7(2)
C	$\frac{2}{3}$	0.0	0.0	0.3075(5)	2.8(4)
N	$\frac{2}{3}$	0.0	0.0	0.1999(5)	2.8(4)

Table S13: Crystallographic details determined by powder X-ray diffraction for $Cu[Co(CN)_6]_{0.67}$ at 3.3 GPa. Thermal parameters and cyanide positions were fixed to the values from the ambient phase.

Formula	$CuCo_{0.67}C_4N_4$				
Space group	$Fm\bar{3}m$				
a (Å)	9.8077(6)				
Z	4				
R_{wp}	0.779%				
Atom	occ	x	y	z	B_{iso} (Å^2)
Cu	1	0.0	0.5	0.0	1.7
Co	$\frac{2}{3}$	0.0	0.0	0.0	1.7
C	$\frac{2}{3}$	0.0	0.0	0.3075	2.8
N	$\frac{2}{3}$	0.0	0.0	0.1999	2.8

5 Phase transitions in $Cu[Pt(CN)_6]$

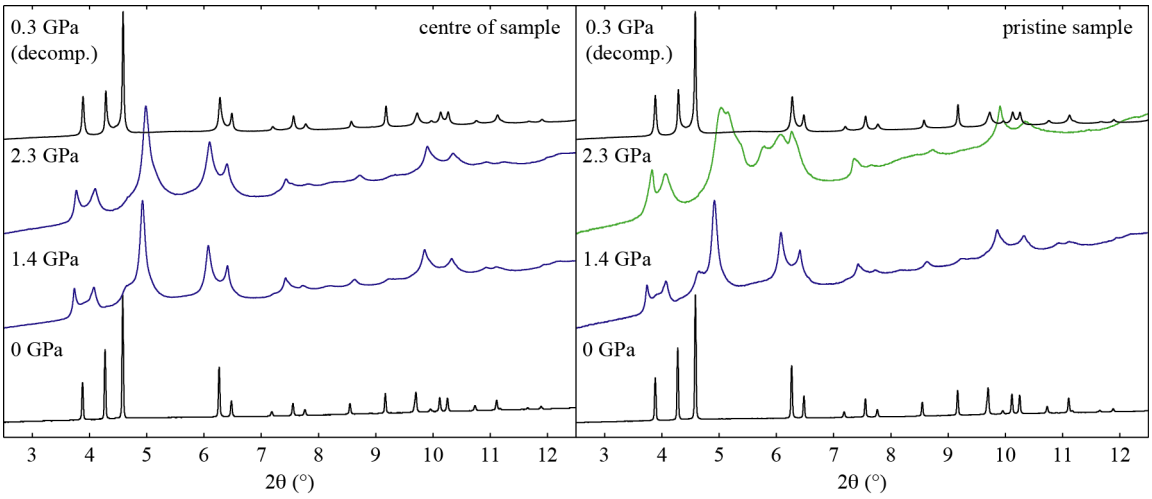

Figure S7: The diffraction patterns of $Cu[Pt(CN)_6]$ ($\lambda = 0.411373$ Å) measured in the centre of the sample and measured at a pristine part of the sample. At 2.3 GPa, the pristine parts of the samples have undergone a second phase transitions not observed in the parts of samples with higher radiation exposure. All phase transitions are fully reversible, as evident in the patterns collected upon decompression.

6 References

(S1) R. J. Angel, M. Alvaro and J. Gonzalez-Platas, *Z. Kristallogr.*, 2014, **229**, 405–419.

(S2) R. J. Angel, *Rev. Mineral. Geochem.*, 2000, **41**, 35–59.

(S3) K. W. Chapman, P. J. Chupas and C. J. Kepert, *J. Am. Chem. Soc.*, 2006, **128**, 7009–7014.